Computers and Geotechnics 37 (2010) 68–81

Contents lists available at ScienceDirect

Computers and Geotechnics

journal homepage: www.elsevier.com/locate/compgeo

Explicit stress integration with error control for the Barcelona Basic Model. Part II: Algorithms efficiency and accuracy

Wojciech T. Sołowski [a,*,1], Domenico Gallipoli [b]

[a] The University of Newcastle, Callaghan NSW 2308, Australia
[b] University of Glasgow, Glasgow G12 8LT, UK

ARTICLE INFO

Article history:
Available online 12 August 2009

Keywords:
Explicit stress integration
Richardson extrapolation
Runge–Kutta methods
Unsaturated soils
Barcelona Basic Model
Elasto-plasticity

ABSTRACT

The paper compares the accuracy and efficiency of explicit stress integration schemes for elasto-plastic unsaturated soil models with automatic error control. Numerical tests are performed with reference to the Barcelona Basic Model (BBM), one of the most popular elasto-plastic models for unsaturated soils, by using eight explicit Runge–Kutta algorithms of various order as well as a novel application of the extrapolation method described in the companion paper. Initially, the results obtained from the lowest order Runge–Kutta scheme (i.e. Modified Euler) as well as the extrapolation method are checked against accurate solutions of a number of BBM paths involving changes of strains and suction. Subsequently, the efficiency and accuracy of all algorithms are assessed for generic increments of strains and suction, while the difference between two alternative error control methods is also analysed. The results presented, although strictly valid for the Barcelona Basic Model, are expected to be general and relevant to other similar unsaturated elasto-plastic models formulated in terms of two independent stress variables such as net stress and suction.

1. Introduction

Stress integration algorithms are a key component of Finite Element routines implementing complex non-linear elasto-plastic models formulated in a differential form. During a Finite Element computation, the stress state is updated at each Gauss point by means of numerical integration of the relevant constitutive model. Given that such operation is repeated a large number of times during one analysis, the accuracy, robustness and efficiency of the integration algorithm are crucially important to the overall performance of the code.

Several alternative approaches are available for numerical integration of elasto-plastic models and, in this work, explicit schemes with automatic error control are considered. In particular, the paper presents results from numerical tests performed by using eight Runge–Kutta pairs described in the companion paper [12], namely the second order Modified Euler scheme [10], the third order Nystrom scheme [5], two Bogacki–Shampine schemes of third and fifth order, respectively [2], a fourth order scheme [5] and three fifth order schemes by England [5,10], Cash–Karp [5,7], and Dormand–Prince [4], respectively. The results from a novel application of the extrapolation method [11] is also presented and compared with the above Runge–Kutta schemes. The two different procedures for error control given in the companion paper [12] – the Error Per Unit Step (EPUS) [8] and the Error Per Step (EPS) [10] – are here assessed in combination with all integration schemes, highlighting the impact that the particular error definition has on the efficiency, accuracy and robustness of the algorithm.

The performance of the different schemes is assessed with specific reference to the integration of the Barcelona Basic Model (BBM) by Alonso et al. [1], which is one of the most popular elasto-plastic models for unsaturated soils. Accuracy is investigated by comparison against rigorous analytical solutions of reference paths in BBM involving changes of strains and suctions that replicate typical laboratory tests as well as by calculating error maps over a range of strain increments. The computational efficiency of the various integration schemes is compared for different magnitudes of the integration error and in conjunction with both EPUS and EPS control.

2. Validation of integration algorithms against analytical reference solutions of BBM

The accuracy of the Runge–Kutta and extrapolation schemes described in the companion paper [12] is assessed through comparison with analytical solutions for a number of BBM reference simulations of typical laboratory tests on unsaturated soil samples. In particular, the following reference simulations have been chosen:

* Corresponding author. Tel.: +61 2 4921 7074; fax: +61 2 4921 6991.
E-mail address: wojciech.solowski@newcastle.edu.au (W.T. Sołowski).
[1] Formerly Durham University, UK.

0266-352X/$ - see front matter © 2009 Elsevier Ltd. All rights reserved.
doi:10.1016/j.compgeo.2009.07.003

(1) Isotropic compression under variable suction (for both isotropic and anisotropic initial stress states).
(2) Oedometric compression under variable suction (for both heavily overconsolidated and slightly overconsolidated soils).
(3) Wetting with impeded volumetric and shear strains (for both isotropic and anisotropic initial stress states).

Consistently with the integration algorithms described in the companion paper [12], the control variable is the increment of strains and suction, i.e. the increment vector of strain with the suction change as an extra component. All reference simulations can be fully described in terms of triaxial stress states, i.e. in terms of stress invariants $\{p, q\}$ where p is the mean net stress and q is the deviator stress. Similarly, the strains and suction increment vector is formulated in terms of strain invariants $\Delta\boldsymbol{\varepsilon}^{\text{enh}} = \{\Delta\boldsymbol{\varepsilon}, \Delta s\} = \{\Delta\varepsilon_s, \Delta\varepsilon_v, \Delta s\}$, where $\Delta\varepsilon_s$ is the increment of shear strain, $\Delta\varepsilon_v$ is the increment of volumetric strain and Δs is the increment of suction.

The BBM parameter values used in the simulations are given in Table 1 and the initial specific volume, v is calculated from the initial stress state according to the following equation:

$$v = N(0) - \lambda(0)\ln\frac{p_0^*}{p^c} - \kappa_s \ln\frac{s + p_{\text{atm}}}{p_{\text{atm}}} - \kappa\ln\frac{p}{p_0^*} \tag{1}$$

where s, p and p_0^* are the initial values of suction, mean net stress and hardening parameter, respectively.

All reference simulations integrate net stresses along a path of strains and suction starting from an elastic initial state and ending at an elasto-plastic final state.

2.1. Analytical solution of BBM

The initial state is defined in terms of specific volume v, mean net stress p, deviator stress q and suction s. The initial value of the hardening parameter is equal to p_0^*, corresponding to a value of the isotropic yield stress at suction s equal to p_0. The elastic increment of strains and suction $\Delta\boldsymbol{\varepsilon}^{\text{enh(e)}}$ is defined as a fraction α of the increment of strains and suction $\Delta\boldsymbol{\varepsilon}^{\text{enh}}$:

$$\Delta\boldsymbol{\varepsilon}^{\text{enh(e)}} = \{\Delta\varepsilon_s^{(e)}, \Delta\varepsilon_v^{(e)}, \Delta s^{(e)}\} = \alpha\Delta\boldsymbol{\varepsilon}^{\text{enh}} = \{\alpha\Delta\varepsilon_s, \alpha\Delta\varepsilon_v, \alpha\Delta s\} \tag{2}$$

Inside the yield locus, increments of strains and suction are rigorously integrated in closed form by solving the system of Eqs. (3)–(6), where the unknowns are the elastic fraction α of the increment of strains and suction, the elastic increment of specific volume $\Delta v^{(e)}$, the increment of mean net stress Δp and the increment of deviator stress Δq.

$$\Delta v^{(e)} = v(e^{-\alpha\cdot\Delta\varepsilon_v} - 1) \tag{3}$$

$$\Delta v^{(e)} = -\kappa\ln\frac{p + \Delta p}{p} - \kappa_s\ln\frac{s + \alpha\Delta s + p_{\text{atm}}}{s + p_{\text{atm}}} \tag{4}$$

$$\Delta q = 3G\alpha\Delta\varepsilon_s \tag{5}$$

$$(q + \Delta q)^2 - M^2(p + \Delta p + ks + k\alpha\Delta s)(p_0 - p - \Delta p) = 0 \tag{6}$$

Note that the solution from Eqs. (3)–(6) is rigorous as the increment of specific volume is obtained in Eq. (3) from the finite increment of volumetric strain.

The elasto-plastic increment of strains and suction $\Delta\boldsymbol{\varepsilon}^{\text{enh(ep)}}$ is given by the remaining fraction $(1 - \alpha)$ of the increment of strains and suction $\Delta\boldsymbol{\varepsilon}^{\text{enh}}$:

$$\begin{aligned}\Delta\boldsymbol{\varepsilon}^{\text{enh(ep)}} &= \{\Delta\varepsilon_s^{(ep)}, \Delta\varepsilon_v^{(ep)}, \Delta s^{(ep)}\} = (1-\alpha)\Delta\boldsymbol{\varepsilon}^{\text{enh}} \\ &= \{(1-\alpha)\Delta\varepsilon_s, (1-\alpha)\Delta\varepsilon_v, (1-\alpha)\Delta s\}\end{aligned} \tag{7}$$

Elasto-plastic increments of strains and suction are integrated starting from the yield state at the end of the elastic increment, defined in terms of specific volume v_y, mean net stress p_y, deviator stress q_y and suction s_y. The integration of the elasto-plastic increment of strains and suction is achieved by solving the system of Eqs. (8)–(18) where Eqs. (16) and (16bis) are used alternatively depending on whether the flow rule is associated or non-associated. In this work, a conventional spreadsheet software is used to solve this system for the eleven unknowns given by the elasto-plastic, elastic and plastic increments of specific volume ($\Delta v^{(ep)}$, $\Delta v^{(e)}$ and $\Delta v^{(p)}$, respectively); the elastic and plastic increments of shear strain and volumetric strain ($\Delta\varepsilon_s^{(e)}, \Delta\varepsilon_s^{(p)}, \Delta\varepsilon_v^{(e)}$ and $\Delta\varepsilon_v^{(p)}$), respectively); the increments of mean net stress and deviator stress (Δp and Δq, respectively); the increment of hardening parameter (Δp_0^*) and the isotropic yield stress (p_0) corresponding to the hardening parameter $p_0^* + \Delta p_0^*$ and suction $s_y + (1 - \alpha)\Delta s$. Note that, the relationship between the finite volumetric strain and the change of specific volume is again used in Eq. (8).

$$\Delta v^{(ep)} = v_y(e^{-(1-\alpha)\Delta\varepsilon_v} - 1) \tag{8}$$

$$\begin{aligned}\Delta v^{(ep)} = N(0) &- \kappa_s\ln\frac{s_y + p_{\text{atm}} + (1-\alpha)\Delta s}{p_{\text{atm}}} \\ &- \lambda[s_y + (1-\alpha)\Delta s]\ln\frac{p_0}{p^c} - \kappa\ln\frac{p_y + \Delta p}{p_0} - v_y\end{aligned} \tag{9}$$

$$(q_y + \Delta q)^2 = M^2(p_y + \Delta p + k(s_y + (1-\alpha)\Delta s))(p_0 - p_y - \Delta p) \tag{10}$$

$$\Delta v^{(e)} = -\kappa\ln\frac{p_y + \Delta p}{p_y} - \kappa_s\ln\frac{s_y + (1-\alpha)\Delta s + p_{\text{atm}}}{s_y + p_{\text{atm}}} \tag{11}$$

$$\Delta v^{(p)} = \Delta v^{(ep)} - \Delta v^{(e)} \tag{12}$$

$$\Delta\varepsilon_v^{(p)} = -\ln\frac{v_y + \Delta v^{(p)}}{v_y} \tag{13}$$

$$\Delta\varepsilon_v^{(e)} = (1-\alpha)\Delta\varepsilon_v - \Delta\varepsilon_v^{(p)} \tag{14}$$

$$\Delta p_0^* = p_0^*\left(e^{\frac{\Delta v^{(p)}}{\kappa - \lambda(0)}} - 1\right) \tag{15}$$

$$\Delta\varepsilon_s^{(p)} = \int_0^{\Delta\varepsilon_v^{(p)}} \frac{\partial Q/\partial q}{\partial Q/\partial q}\,\mathrm{d}\varepsilon_v^{(p)} = \int_0^{\Delta\varepsilon_v^{(p)}} \frac{2q}{M^2(2p + ks - p_0)}\,\mathrm{d}\varepsilon_v^{(p)} \tag{16}$$

Table 1
BBM parameter values.

Parameter	Description	Value	Aspect of soil behaviour
κ	Swelling index for changes in mean net stress	0.02	Elastic behaviour
κ_s	Swelling index for changes in suction	0.008	
G (MPa)	Shear modulus	20	
p_{atm} (kPa)	Atmospheric pressure	100	
$\lambda(0)$	Slope of NCL at zero suction	0.2	Plastic behaviour
r	Parameter controlling ratio of NCL slopes at $s \to \infty$ and $s = 0$	0.75	
β (kPa^{-1})	Parameter controlling variation of NCL slope with suction	0.01	
p_c (kPa)	Reference pressure	10	
k	Parameter controlling cohesion increase with suction	0.6	Strength behaviour
M	Slope of critical state line in constant suction planes	0.5	

$$\Delta\varepsilon_s^{(p)} = \int_0^{\Delta\varepsilon_v^{(p)}} \frac{\partial Q/\partial q}{\partial Q/\partial q} \mathrm{d}\varepsilon_v^{(p)} = \frac{\lambda(0)}{\lambda(0)-\kappa} \int_0^{\Delta\varepsilon_v^{(p)}} \frac{2M(M-9)(M-3)q}{9(6-M)M^2(2p+ks-p_0)} \mathrm{d}\varepsilon_v^{(p)} \quad (16\text{bis})$$

$$\Delta\varepsilon_s^{(e)} = (1-\alpha)\Delta\varepsilon_s - \Delta\varepsilon_s^{(p)} \quad (17)$$

$$\Delta q = 3G\Delta\varepsilon_s^{(e)} \quad (18)$$

Inspection of the system of Eqs. (8)–(18) indicates that all unknowns can be calculated by closed form expressions with the exception of the increment of plastic shear strain, which is given by the integral of Eq. (16) or (16bis). The value of such integral depends on the particular stress path followed during the increment and can only be calculated rigorously in special cases (e.g. when the integrand is constant) and is most often replaced by an approximate numerical integration. Whenever necessary in the reference simulations described below, the increment of plastic shear strain has been approximately calculated by explicit Euler integration as:

$$\Delta\varepsilon_s^{(p)} \cong \frac{2q}{M^2(2p+ks-p_o)}\Delta\varepsilon_v^{(p)} \quad (19)$$

$$\Delta\varepsilon_s^{(p)} \cong \frac{\lambda(0)}{\lambda(0)-\kappa}\frac{2M(M-9)(M-3)q}{9(6-M)M^2(2p+ks-p_o)}\Delta\varepsilon_v^{(p)} \quad (19\text{bis})$$

In this case, an accurate solution, is obtained by splitting the elasto-plastic increment of strains and suction in small equal subincrements and by solving, for each subincrement, the above system of equations where (16) and (16bis) are replaced by (19) and (19bis), respectively. The solution is considered accurate when the solutions obtained with doubled number of subincrements differ only in the seventh significant digit.

2.2. Isotropic compression under variable suction

Isotropic compression paths are simulated by using the previous analytical solution as well as the integration schemes described in the companion paper [12]. In particular, three different compression paths are simulated through the integration of a sequence of progressively larger increments of strains and suction of the form $\Delta\boldsymbol{\varepsilon}^{enh} = \{0, \Delta\varepsilon_v, \Delta s\}$. Each increment is defined by proportional changes of volumetric strain and suction up to a maximum volumetric strain of 15% and maximum suction changes of −50 kPa, 100 kPa and zero, respectively. In this way, the accuracy of the integration schemes is also tested with reference to increments of different sizes.

Simulations are calculated for two different initial stress states: an isotropic stress state corresponding to a mean net stress of 15 kPa as well as an anisotropic stress state corresponding to a mean net stress and a deviator stress of 15 kPa and 30 kPa, respectively. In all tests, the initial value of suction is taken equal to 100 kPa and the initial value of the hardening parameter is taken equal to 50 kPa.

In the case of the isotropic initial stress state, the increment of deviator stress is zero (as there is no plastic or elastic shear strain) and, therefore, the elasto-plastic increments of strains and suction can be rigorously integrated by using Eqs. (8)–(15). In the case of an anisotropic initial stress state, the shear strains are non-zero during elasto-plastic loading and the full system of Eqs. (8)–(18) must be used instead.

Fig. 1a and b shows the simulations corresponding to the different suction increments in the p–s and ε_v–p planes, respectively, for the case of an isotropic initial stress state. In these figures, the analytical solution is compared with the numerical integrations performed by using both the lowest order Runge–Kutta scheme (i.e. Modified Euler) and the extrapolation method introduced in the companion paper [12]. For simplicity, in this section as well as in the following sections, the analytical solution is only compared with the lowest order Modified Euler Runge–Kutta scheme but similar conclusions can be drawn for the higher order Runge–Kutta schemes. Given that the curves in Fig. 1 (and in the following Figs. 2–8) are obtained by integrating progressively larger increments from the same initial state, the maximum absolute error tends to grow as the strain increases but the maximum percentage error remains fairly constant.

Simulations for the case of an anisotropic initial stress state are shown in the p–q and ε_v–p planes with both associated (Fig. 2a and b) and non-associated (Fig. 3a and b) flow rules.

An integration tolerance of 20% (used in conjunction with the EPS control) is set for both the Modified Euler and extrapolation methods. Despite such relatively high tolerance, numerical integration by these two schemes provides a very good match with the reference analytical solutions and the errors remain significantly smaller than the set tolerance. The only exception to this general trend is the result provided by the extrapolation method for the simulation starting from an initial anisotropic stress state with an associated flow rule shown in Fig. 2b. In this particular case, oscillations of deviator stress are observed after the stress state has become isotropic towards the end of the stress path. Although these oscillations seem very large relative to the level of deviator stress, the absolute magnitude of the error in deviator stress is the same as the error in mean net stress. This was the only case observed where the extrapolation method appeared to provide less accurate results than algorithms based on Runge–Kutta methods.

2.3. Oedometric loading under variable suction

Three oedometric compression paths are simulated by integration of a sequence of progressively larger increments of strains and suction of the form $\Delta\boldsymbol{\varepsilon}^{enh} = \{\Delta\varepsilon_v, 2/3\Delta\varepsilon_v, \Delta s\}$. In each increment, proportional changes of volumetric strain and suction are assumed up to a maximum volumetric strain of 15% and maximum suction changes of −50 kPa, 100 kPa and zero, respectively. Note that the shear strain increment is equal to 2/3 of the volumetric strain increment as required under oedometric conditions.

The initial value of suction is equal to 100 kPa and the initial value of the hardening parameter is equal to 200 kPa in all simulations. Two different isotropic initial stress states are considered corresponding to a highly overconsolidated soil, with an initial mean net stresses of 5 kPa, and a slightly overconsolidated soil, with an initial mean net stress of 200 kPa.

Oedometric compression generates shear strains and the full system of Eqs. (8)–(18) must, therefore, be solved in order to obtain the analytical solution in the plastic domain.

The simulations corresponding to the different suction increments for the case of a highly overconsolidated soil with associated and non-associated flow rule are given in Figs. 4 and 5, respectively. In particular, Figs. 4a and 5a show the simulations in the p–q plane whereas Figs. 4b and 5b show the same simulations in the ε_v–p plane. Similar simulations for the case of a slightly overconsolidated soil with associated and non-associated flow rule are given in Figs. 6 and 7, respectively.

The stress paths starting from a highly overconsolidated state yield on the dry side of the plastic surface whereas the stress paths starting from a slightly overconsolidated state yield on the wet side. Inspection of Figs. 4–7 indicates that, despite the relatively large integration tolerance of 20% (used in conjunction with the EPS control), the integration from the extrapolation algorithm is almost undistinguishable from the analytical solution except for the

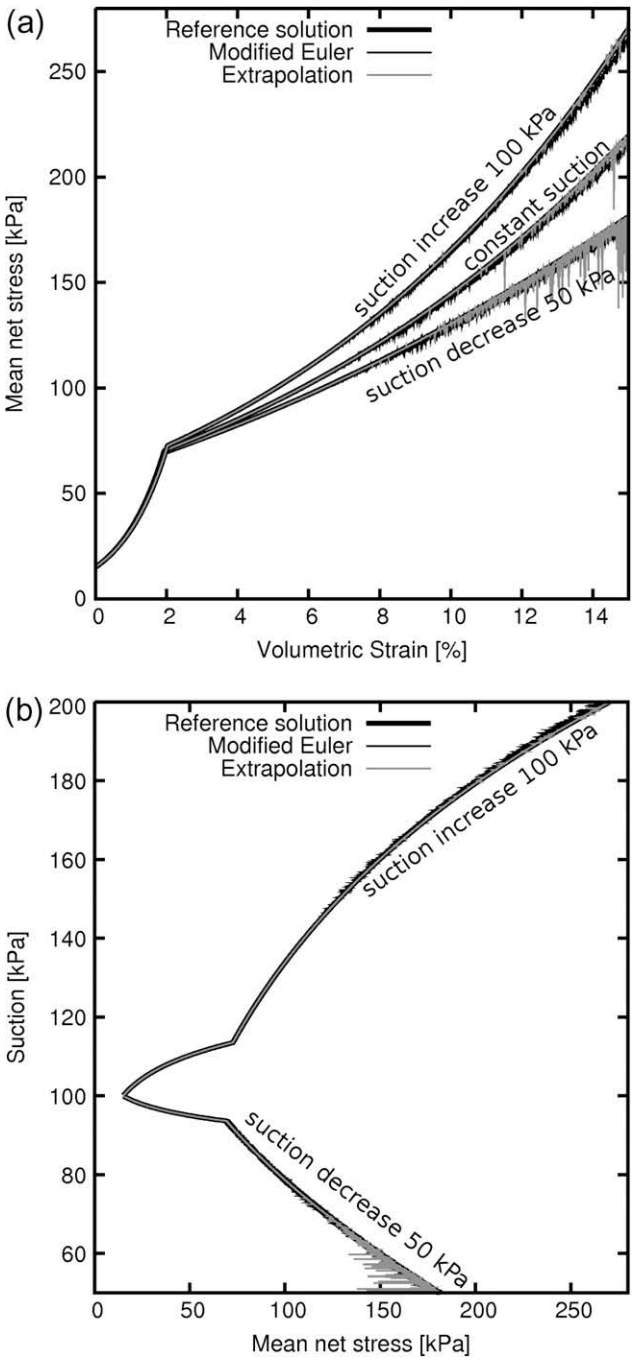

Fig. 1. Isotropic loading at variable suction starting from an initial isotropic stress state: (a) mean net stress versus volumetric strain and (b) suction versus mean net stress.

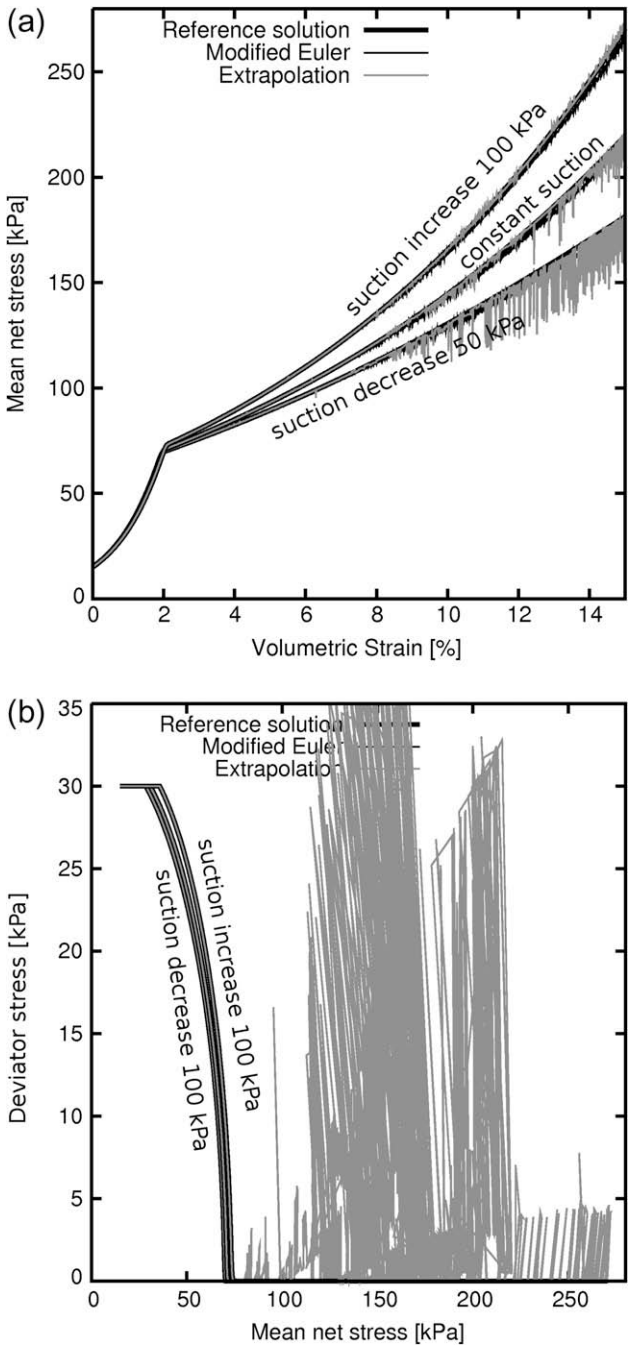

Fig. 2. Isotropic loading at variable suction starting from an initial anisotropic stress state with associated flow rule: (a) mean net stress versus volumetric strain and (b) deviator stress versus mean net stress.

relatively small oscillations in Figs. 4 and 6 limited to the final part of the simulation with a reduction of suction of 50 kPa. On the other hand, inspection of Figs. 4–7 suggests that the integration error from the Modified Euler algorithm is in general significantly larger than that observed for the extrapolation algorithm but still considerably smaller than the integration tolerance of 20%.

2.4. Wetting with impeded volumetric and shear strains

Wetting with impeded volumetric and shear strains is simulated by integration of a sequence of progressively larger increments of the form $\Delta\boldsymbol{\varepsilon}^{\text{enh}} = \{0, 0, \Delta s\}$ up to a maximum suction change of −100 kPa. Two different initial stress states are considered: an isotropic stress state corresponding to a mean net stress of 70 kPa as well as an anisotropic stress state corresponding to a mean net stress and a deviator stress of 15 kPa and 30 kPa, respectively. The initial values of suction and hardening parameter are taken equal to 100 kPa and 50 kPa, respectively.

For the simulation with an isotropic initial stress state, the increments of deviator stress, plastic shear strain and elastic shear strain are all zero and the elasto-plastic increments of strains and suction are, therefore, rigorously integrated by using Eqs. (8)–(15).

Fig. 8a shows the simulations in the s–p plane for the cases of an initially isotropic stress state, an initially anisotropic stress state

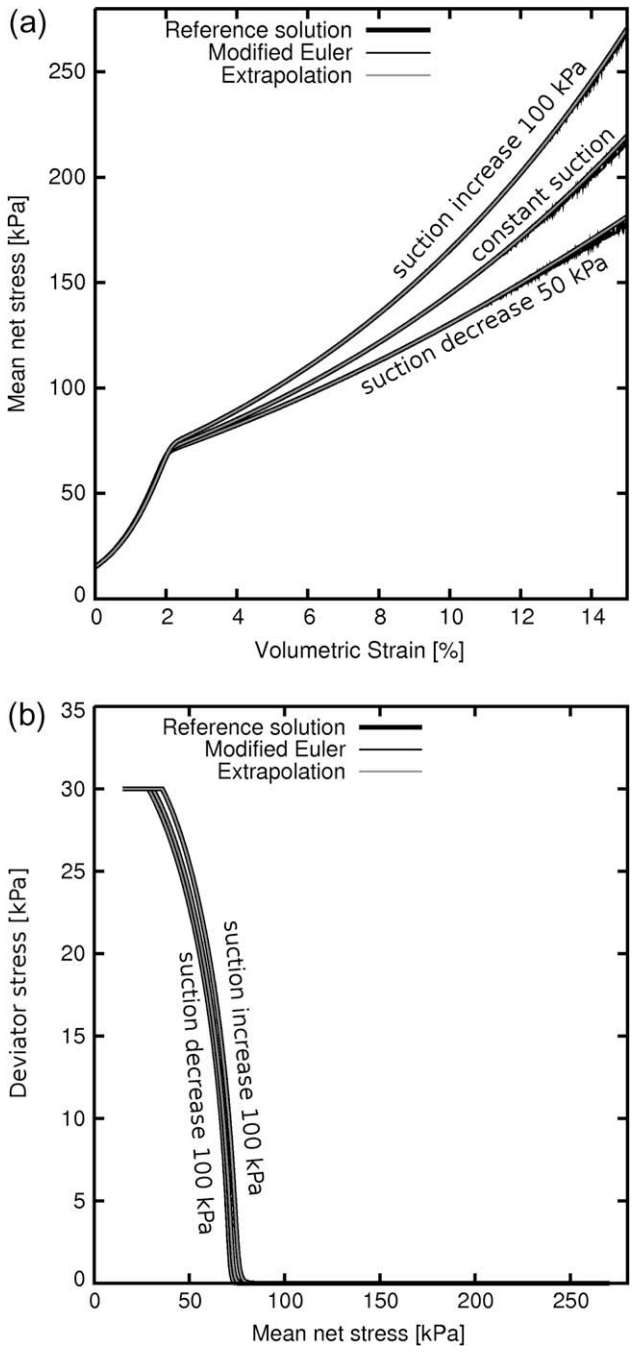

Fig. 3. Isotropic loading at variable suction starting from an initial anisotropic stress state with non-associated flow rule: (a) mean net stress versus volumetric strain and (b) deviator stress versus mean net stress.

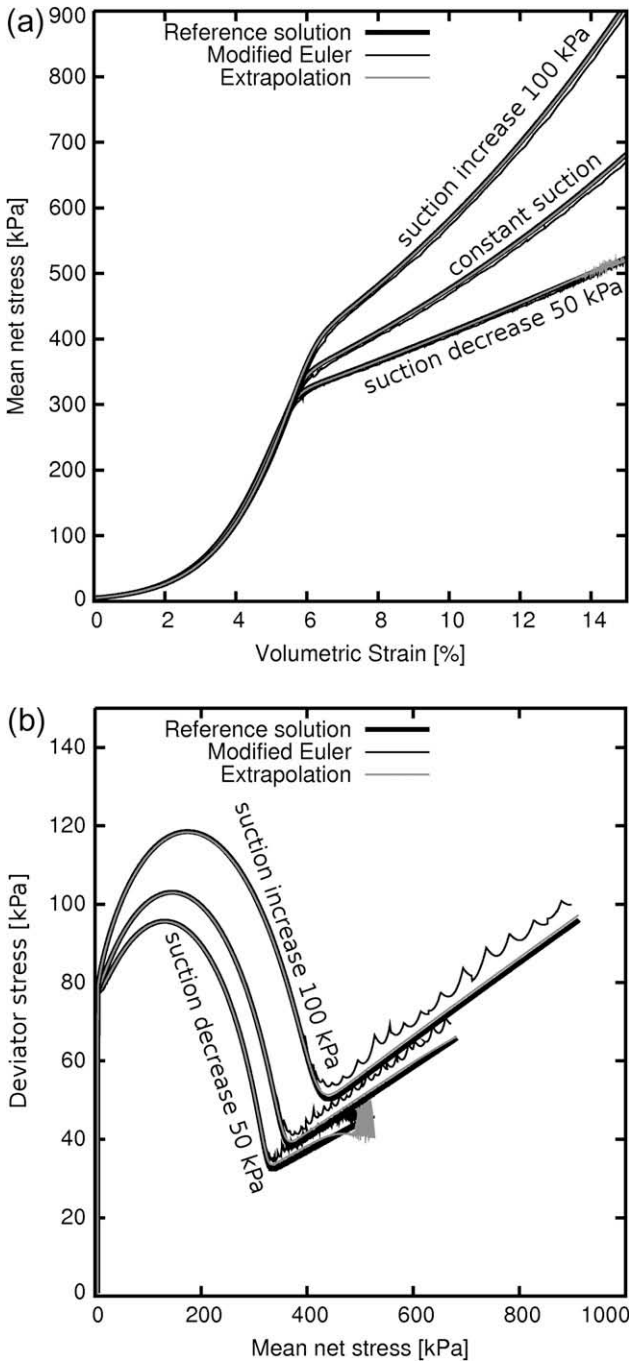

Fig. 4. Oedometric loading at variable suction for heavily overconsolidated soil with associated flow rule: (a) mean net stress versus volumetric strain and (b) deviator stress versus mean net stress.

with associated flow rule and an initially anisotropic stress state with non-associated flow rule. Fig. 8b shows the reference simulations in the p–q plane for the case of an initially anisotropic stress state with both associated and non-associated flow rule.

Note that, in both Figs. 8a and b, the curves corresponding to associate and non-associate flow rules virtually overlap and are impossible to differentiate. It is also interesting to note in Fig. 8b that the small oscillation towards the end of the curve calculated by the Modified Euler algorithm (around a value of mean net stress of 19 kPa) is obtained with almost exactly similar characteristics regardless of whether an associated or a non-associated flow rule is chosen.

Similarly to previous simulations, the error made by the Modified Euler and extrapolation algorithms is markedly smaller than the integration tolerance of 20% used during numerical integration in conjunction with the EPS control. The integration by the extrapolation method is almost indistinguishable from the analytical solution while the results from the Modified Euler show only a very slight departure from the analytical solution.

3. Efficiency and accuracy of proposed stress integration schemes

The efficiency of the various stress integration schemes has been compared in terms of the computational time required to

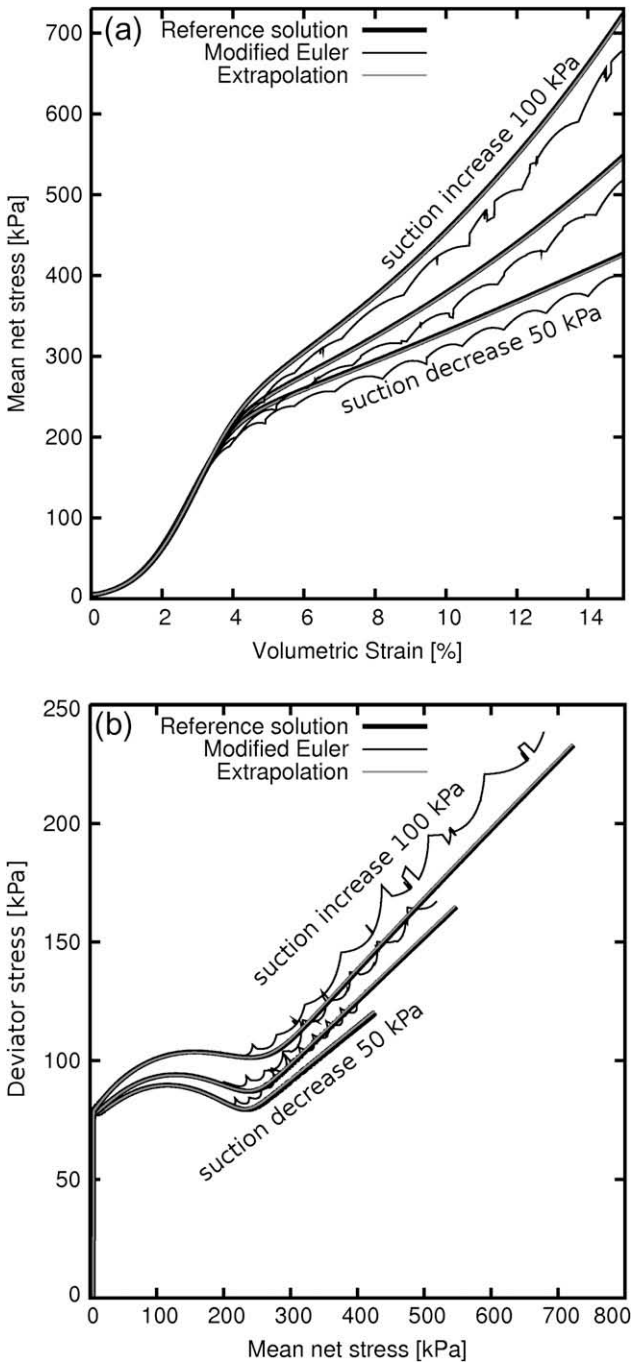

Fig. 5. Oedometric loading at variable suction for heavily overconsolidated soil with non-associated flow rule: (a) mean net stress versus volumetric strain and (b) deviator stress versus mean net stress.

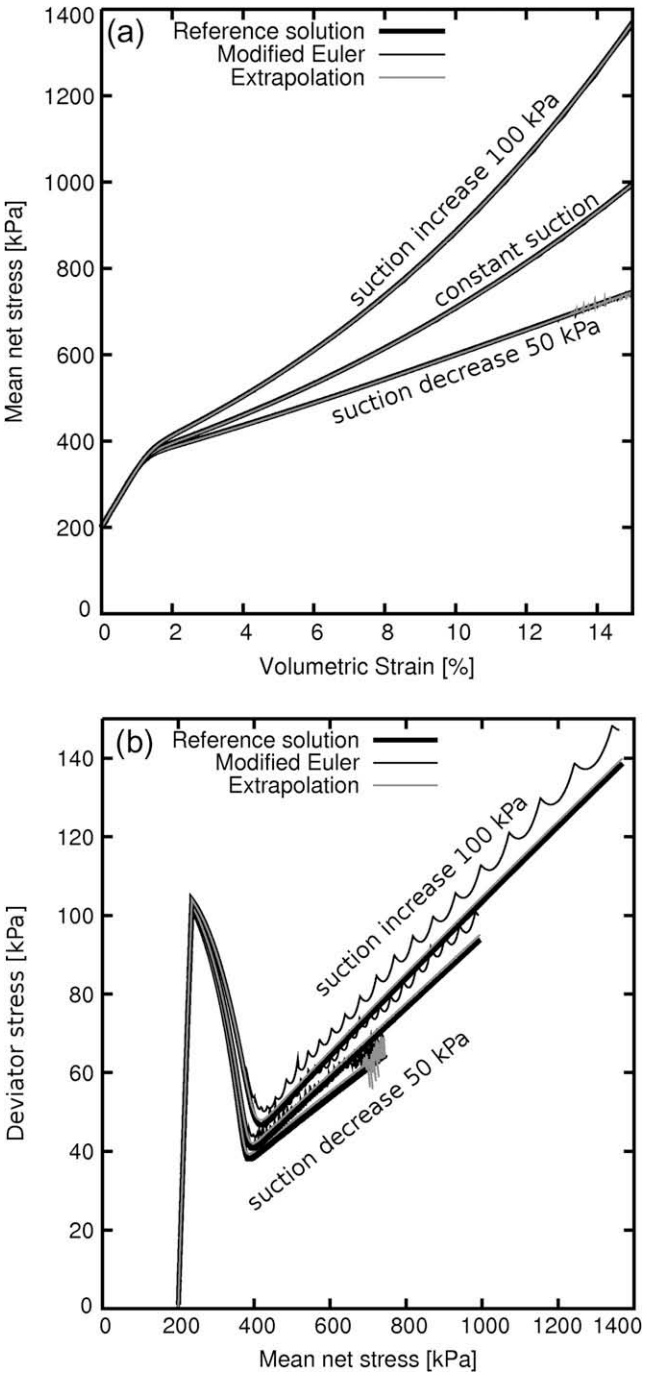

Fig. 6. Oedometric loading at variable suction for slightly overconsolidated soil with associated flow rule: (a) mean net stress versus volumetric strain and (b) deviator stress versus mean net stress.

integrate a large set of increments of strains and suction with different average integration errors.

All nine integration schemes have been used to calculate the net stress increments $\Delta\boldsymbol{\sigma} = \{\Delta\sigma_{11}, \Delta\sigma_{22}, \Delta\sigma_{33}, \Delta\sigma_{12}, \Delta\sigma_{13}, \Delta\sigma_{23}\}$ corresponding to 6000 different increments of strains and suction randomly generated in the seven-dimensional space $\Delta\boldsymbol{\varepsilon}^{\text{enh}} = \{\Delta\varepsilon_{11}, \Delta\varepsilon_{22}, \Delta\varepsilon_{33}, \Delta\varepsilon_{12}, \Delta\varepsilon_{13}, \Delta\varepsilon_{23}, \Delta s\}$. Normal strains $\Delta\varepsilon_{11}$, $\Delta\varepsilon_{22}$ and $\Delta\varepsilon_{33}$ have been randomly generated over the interval [−5%; 5%], shear strains $\Delta\varepsilon_{12}$, $\Delta\varepsilon_{13}$ and $\Delta\varepsilon_{23}$ over the interval [−3%; 3%] and suction increment Δs over the interval [−100 kPa; 200 kPa]. The same isotropic initial stress state is assumed for all increments, with values of mean net stress, suction and hardening parameter equal to 350 kPa, 100 kPa and 200 kPa, respectively. The isotropic yield stress p_0 corresponding to the initial suction of 100 kPa is, therefore, calculated as 379 kPa. The BBM parameter values used in the integration are listed in Table 1.

For comparison, reference quasi-rigorous net stress increments $\Delta\boldsymbol{\sigma}^{(\text{ref})} = \left\{\Delta\sigma_{11}^{(\text{ref})}, \Delta\sigma_{22}^{(\text{ref})}, \Delta\sigma_{33}^{(\text{ref})}, \Delta\sigma_{12}^{(\text{ref})}, \Delta\sigma_{13}^{(\text{ref})}, \Delta\sigma_{23}^{(\text{ref})}\right\}$ were also calculated for each increment of strains and suction. The accuracy of the reference solution was ensured by dividing each increment in 10E+6 equal sized subincrements and using explicit Euler integration to calculate stresses over each small subincrement. To minimise the errors due to machine accuracy a 30 digits storage was used to calculate the reference net stress increment $\Delta\boldsymbol{\sigma}^{(\text{ref})}$.

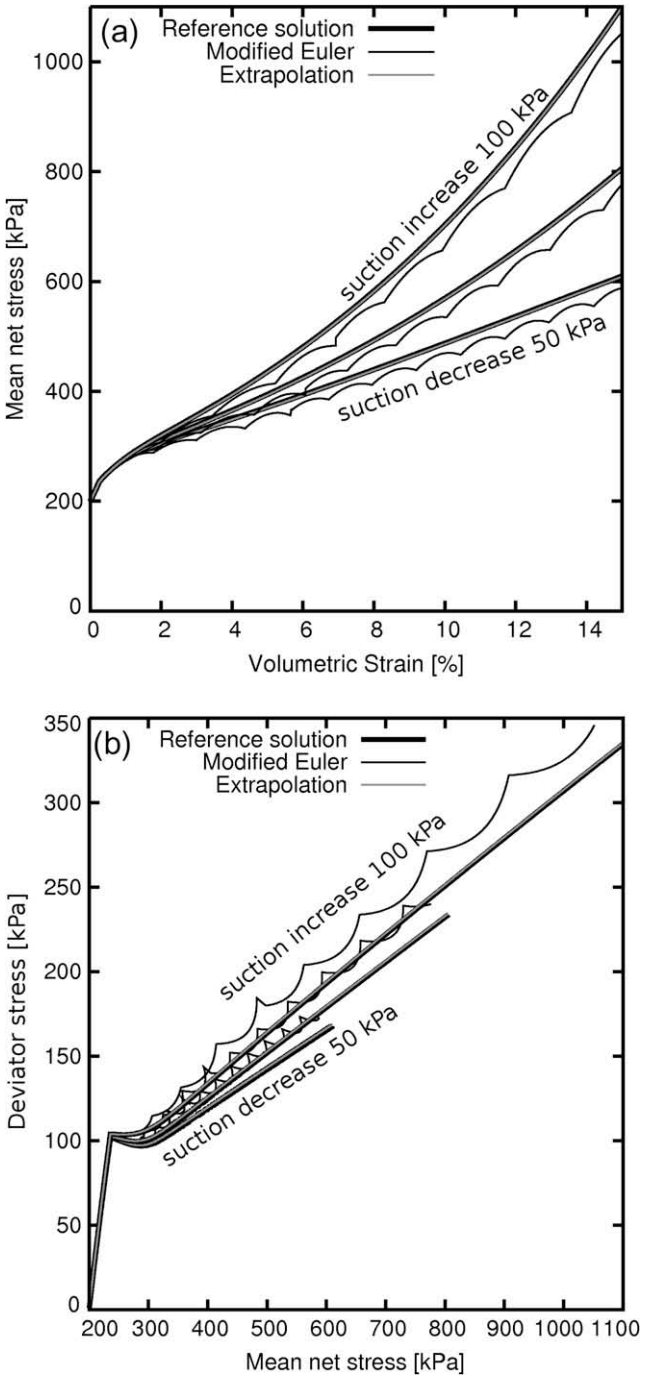

Fig. 7. Oedometric loading at variable suction for slightly overconsolidated soil with non-associated flow rule: (a) mean net stress versus volumetric strain and (b) deviator stress versus mean net stress.

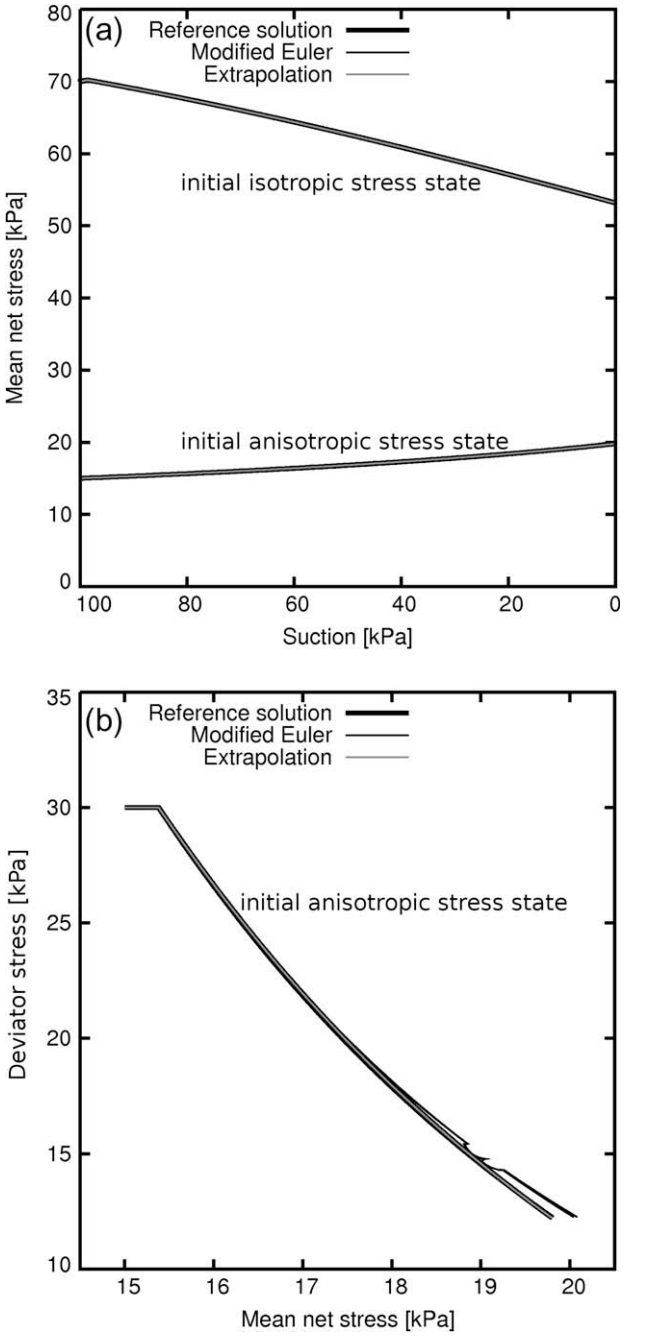

Fig. 8. Wetting with impeded volumetric and shear strains starting from both initial isotropic and anisotropic stress states and with both associated and non-associated flow rule: (a) mean net stress versus suction and (b) deviator stress versus mean net stress. Note that simulations with associated and non-associated flow rule virtually overlap.

The error of the different integration schemes was quantified against this reference solution by calculating the average relative error E_{av} (i.e. the average relative error for individual net stress components and for all random increments of strains and suction – see also [11]) as:

$$E_{av} = \frac{1}{6000}\sum_{n=1}^{6000}\frac{1}{6}\left(E_{11}^{(n)} + E_{22}^{(n)} + E_{33}^{(n)} + E_{12}^{(n)} + E_{13}^{(n)} + E_{23}^{(n)}\right) \tag{20}$$

where $E_{ij}^{(n)}$ is the relative error of the ijth component of the net stress increment corresponding to the integration of the nth increment of strains and suction among the set of 6000 random generations and is defined as:

$$E_{ij}^{(n)} = \frac{|\Delta\sigma_{ij} - \Delta\sigma_{ij}^{(ref)}|}{\Delta\sigma_{ij}^{(abs)}} \quad i,j = 1,2,3 \tag{21}$$

where $\Delta\sigma_{ij}$ is the net stress increment computed by the relevant integration scheme, $\Delta\sigma_{ij}^{(ref)}$ is the reference net stress increment and $\Delta\sigma_{ij}^{(abs)}$ is the sum of the absolute values of the net stress subincrements computed by the explicit Euler integration in each of the 10E+6 substeps of the reference solution. The quantity $\Delta\sigma_{ij}^{(abs)}$ is

used instead of $\Delta\sigma_{ij}^{(\mathrm{ref})}$ in order to provide a better approximation of the relative error. Otherwise, it might happen that, for a given increment of strains and suction, one or more components of the reference net stress increment $\Delta\sigma_{ij}^{(\mathrm{ref})}$ (calculated as the sum of the relevant 10E+6 subincrements) are close to zero and the calculated error value would be very high even for a relatively accurate solution.

Fig. 9 compares efficiency of different Runge–Kutta schemes in conjunction with both EPS and EPUS error control. In particular, Fig. 9 shows the relationship between computation time and average error, calculated according to Eq. (20), for the second order Modified Euler scheme, the best performing third order scheme (i.e. Nystrom), the fourth order scheme and the best performing fifth order scheme (i.e. Cash–Karp), where each curve has been obtained by running the relevant algorithm with different integration tolerances.

For the two lower order schemes, there is a clear tendency of the computational time to increase when the average error decreases, as expected. However, the two higher order schemes show only a slight variation of computation time when average errors change several orders of magnitude. In particular, a counterintuitive decrease of computational time with decreasing average error is initially observed. This behaviour (especially evident in Fig. 9a where EPS is used) is caused by plastic drift occurring at the end of some substeps, which requires mapping the stress state back to the yield locus as described in the companion paper [12]. Each drift correction is added to the estimated error leading to larger numbers of rejected substeps and hence longer computation times when

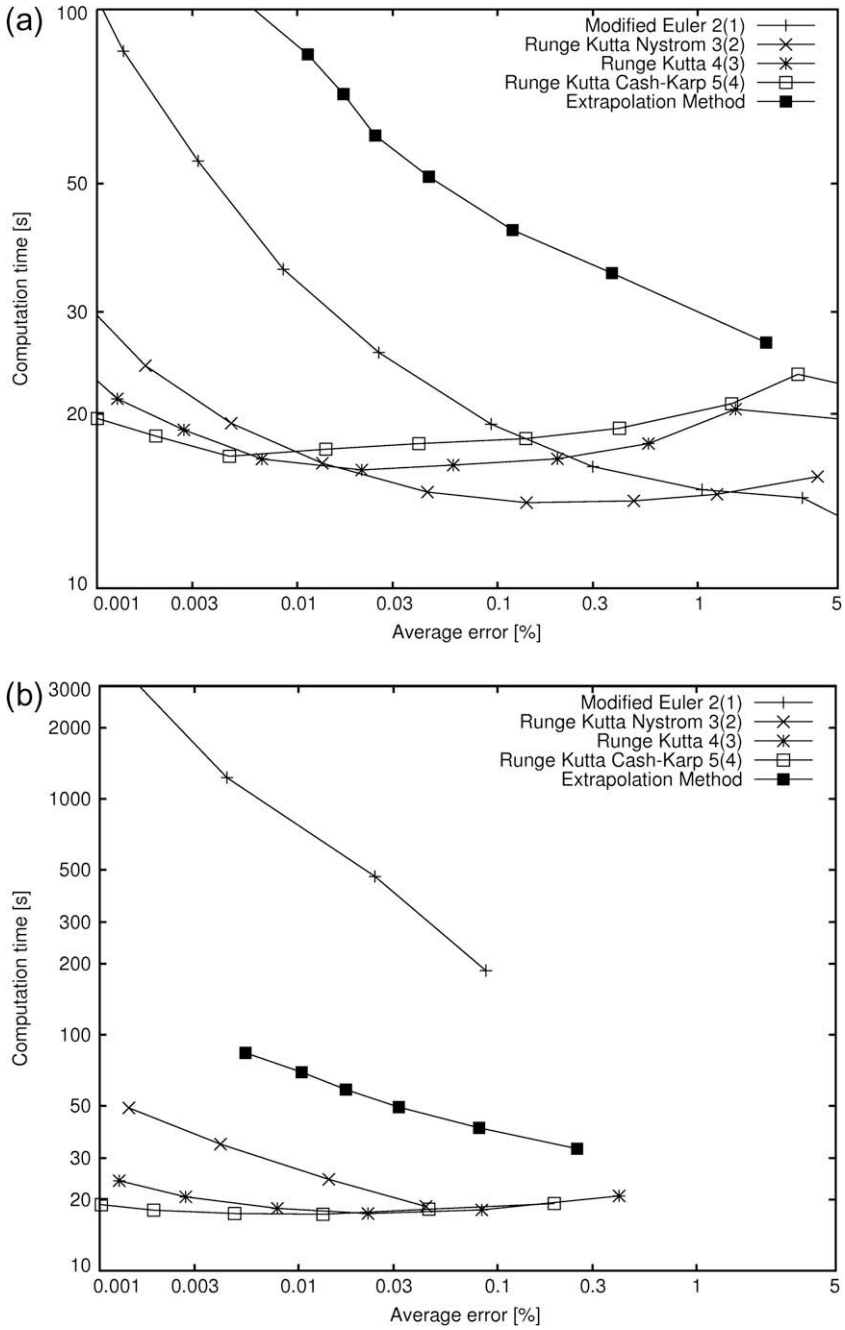

Fig. 9. Computation time against average error of Runge–Kutta schemes in conjunction with: (a) EPS control and (b) EPUS control.

lenient tolerances are used (i.e. at high values of the average error). On the other hand, the drift correction becomes largely irrelevant when the integration tolerance is stricter.

Inspection of Fig. 9a indicates that, when EPS is used, the Modified Euler is the most efficient scheme for very crude accuracies while higher order schemes become more competitive as the average error decreases. Overall, the third order Nystrom scheme appears the best for the range of average errors considered. This scheme remains competitive even for relatively stringent accuracies and is outperformed by the fourth order scheme and fifth order Cash–Karp scheme only when the average error decreases to about 0.01%. The extrapolation scheme appears significantly slower than any Runge–Kutta scheme.

When EPUS is used, the extrapolation method is no longer the slowest scheme and the Modified Euler exhibits the poorest efficiency as shown in Fig. 9b. In general the efficiency worsens for Runge–Kutta methods whereas it remains largely unchanged for the extrapolation method. Comparison between Fig. 9a and b indicates that the loss of efficiency for Runge–Kutta methods mainly affects the lower order schemes. For the fourth order scheme and the fifth order Cash–Karp scheme the computation times remain virtually the same regardless whether the EPS or EPUS control is used. In addition, when EPUS control is used, the fourth order scheme and the fifth order Cash–Karp scheme are the most efficient choices throughout the whole range of accuracies. The Cash–Karp scheme is the most efficient scheme when very high accuracy is required, regardless whether it is used in conjunction with EPS or EPUS control. It is important to note, however, that the convergence of Runge–Kutta schemes tends to deteriorate especially when low values of the integration tolerance, i.e. below 0.1%, are chosen.

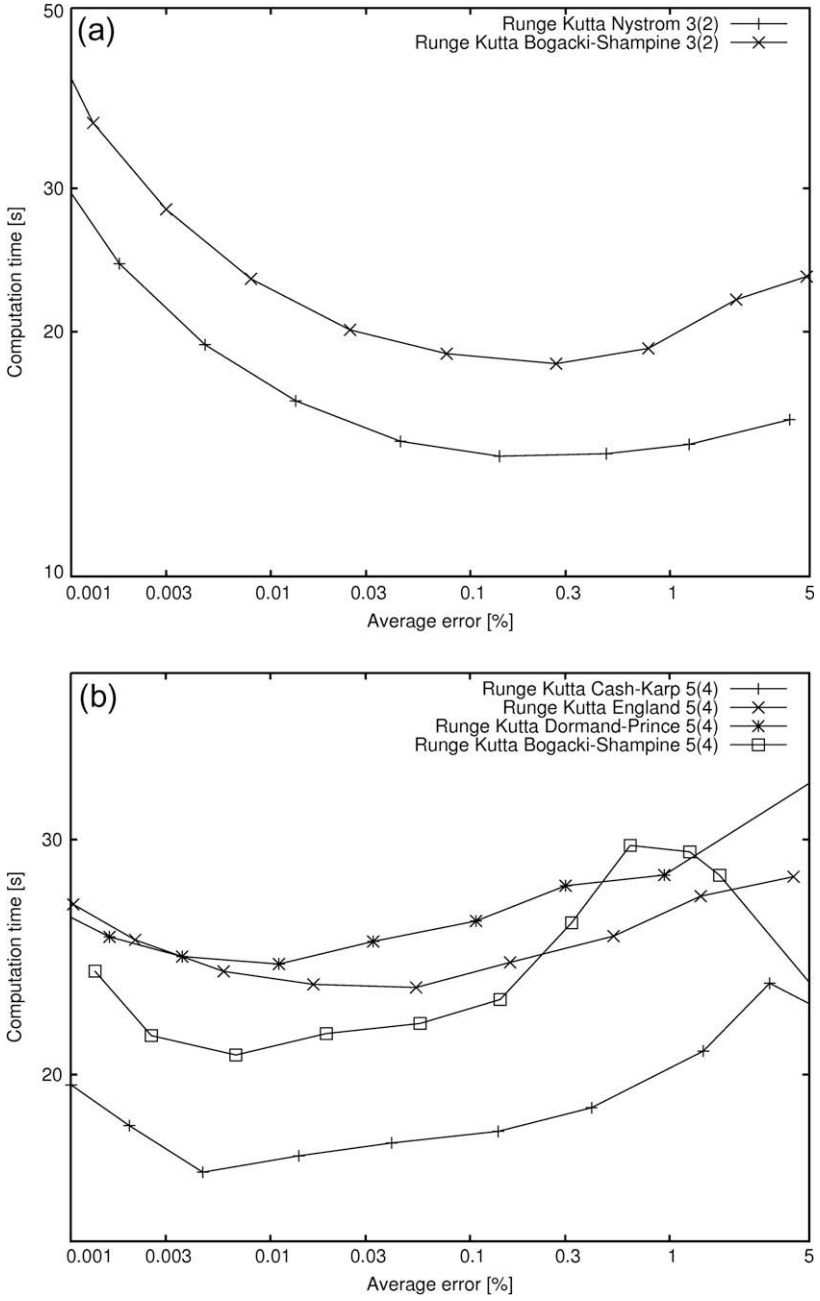

Fig. 10. Computation time against average error for Runge–Kutta schemes of: (a) third order and (b) fifth order.

Fig. 10a compares efficiency of the two third order schemes (i.e. the Nystrom and Bogacki–Shampine schemes) while Fig. 10b presents similar comparisons for the four fifth order schemes (i.e. the Bogacki–Shampine, England, Cash–Karp and Dormand–Prince schemes). The results presented in both figures refer to the case where EPS control is used but similar behaviour is obtained for EPUS control. Inspection of both figures indicates that the recently proposed Bogacki–Shampine third order and fifth order schemes are noticeably less efficient than the third order Nystrom and fifth order Cash–Karp schemes, respectively. This is partly because both these Bogacki–Shampine schemes do not benefit from the use of the FSAL (First Same As Last) technique, which is one of their main advantages. The FSAL technique allows saving one evaluation of the elasto-plastic stiffness matrix by using the last evaluation within a successful substep as the first evaluation of the following substep. The FSAL technique is not implemented here because the stress state at the end of a given substep might change due to drift correction, so the last evaluation of the elasto-plastic matrix might no longer be relevant to the stress state at the start of the subsequent substep. A partial implementation of the FSAL technique was, however, tested whereby the last evaluation of the elasto-plastic stiffness matrix is used again in the subsequent substep in case no drift correction was performed and this only led to slightly better performance.

Fig. 11 compares the relationship between average error, calculated according to Eq. (20), and the corresponding integration tol-

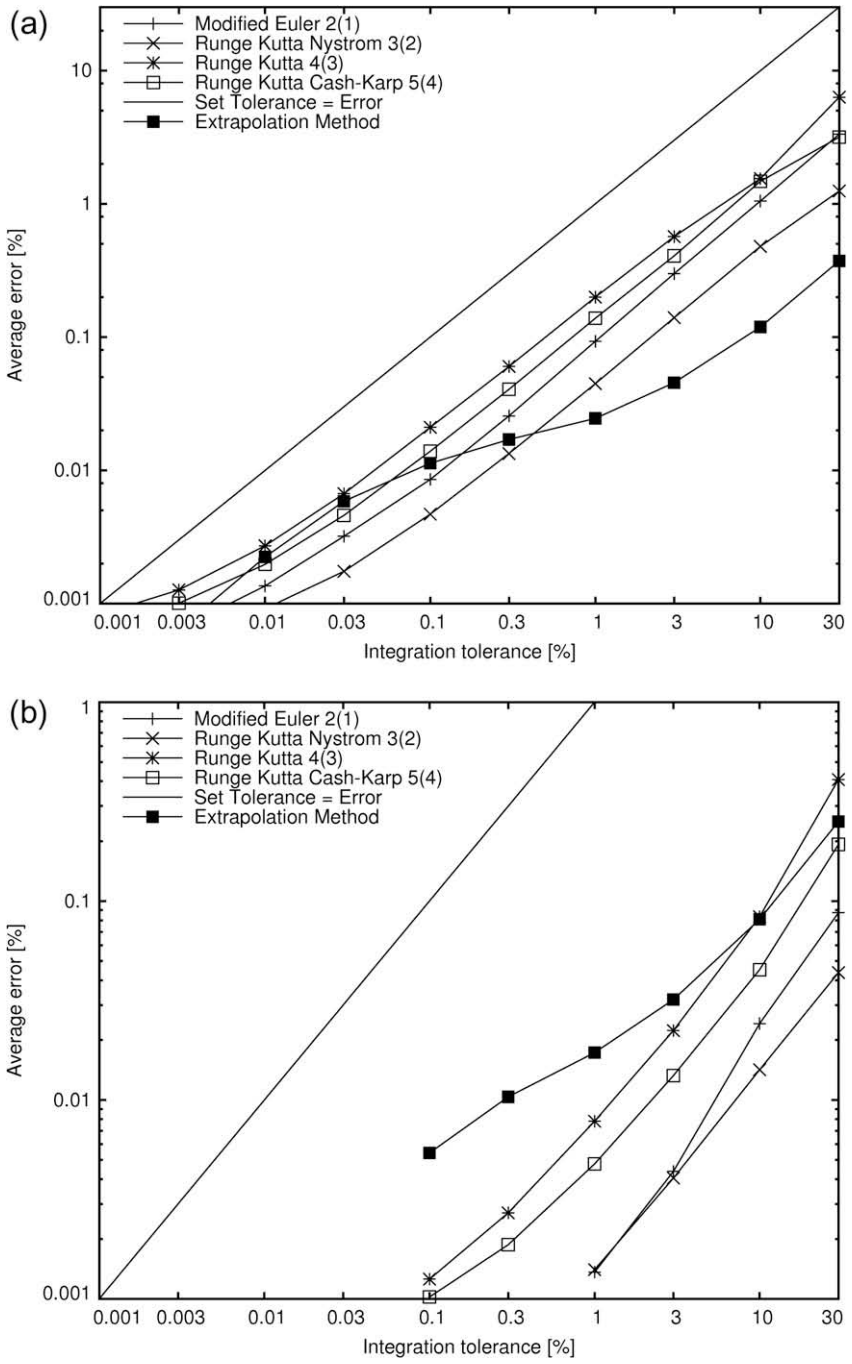

Fig. 11. Average error against integration tolerance of Runge–Kutta schemes in conjunction with: (a) EPS control and (b) EPUS control.

erance for the same schemes shown in Fig. 9. It can be noticed that the average error is considerably smaller than the set tolerance for all schemes. This is not surprising as it has already been shown in the previous section that the integration errors of Modified Euler and extrapolation schemes, evaluated against analytical solutions, are significantly smaller than the set tolerance. Comparison of Fig. 11a and b also indicates that, for all Runge–Kutta schemes, the difference between the average error and the set tolerance increases when the EPUS method is used resulting in significantly more accurate integration than required. This is due to the stricter error control imposed by the EPUS method whereby the error in each substep is estimated relative to the corresponding stress increment (rather than relative to the current stress value, as it is the case for the EPS method). For the extrapolation scheme, the difference between the average error and the set tolerance is still significant but, unlike the Runge–Kutta schemes, it does not appear to be influenced by the particular choice of error control.

Inspection of Fig. 11 also indicates that, for Runge–Kutta schemes, the relationship between the logarithm of the average error and the logarithm of the integration tolerance is reasonably parallel to the identity line. The results shown here refer to large strain increments, so each substep is expected to be close to the optimal size. However, previous Finite Element analyses of boundary value problems (see e.g. [10,9,6]) show that, even when suboptimal substep sizes occur in conjunction with EPS control, the error remains smaller than the set tolerance and varies proportionally in a logarithmic plane with the tolerance value, as expected for strictly dissipative systems [3]. Fig. 11 also shows that, when the extrapolation method is used, the difference between the logarithm of the average error and the logarithm of the integration tolerance is no longer constant as for Runge–Kutta schemes, but it tends to reduce when the average error decreases.

It is important to note that, in spite of the relatively low efficiency, the extrapolation method appears the most robust integration scheme showing virtually no failure to converge for all increments of strains and suction, regardless whether EPS or EPUS control is used. This is because the extrapolation method is based on a global error estimate, which is advantageous in terms of numerical stability with respect to the local error estimate used by Runge–Kutta schemes. As described in the companion paper [12], the extrapolation method is nothing else than a numerical technique to improve, through subsequent extrapolations, the convergence rate of a given explicit integration algorithm. Hence, the robustness of the extrapolation method will not be worse than that of the chosen explicit integration algorithm.

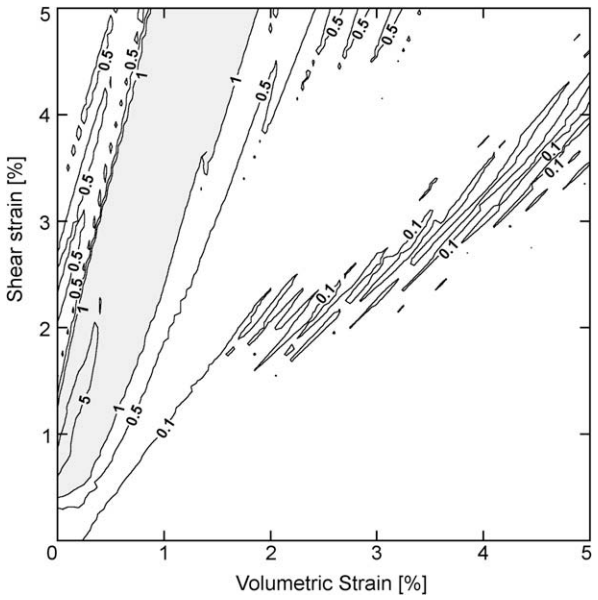

Fig. 12. Map of maximum integration errors produced by the Modified Euler second order Runge–Kutta scheme in conjunction with EPS control. Areas with errors larger than the set tolerance of 1% are greyed out.

It is worth reinstating here that the errors shown in Fig. 11 are average values calculated by Eq. (20) over all net stress components and across 6000 increments of strains and suction. The integration error for an individual increment of strains and suction might be quite different from such average values as it will be shown in the next section, where the accuracy of each integration scheme is studied in greater detail by mapping errors over the strain space.

4. Iso-error maps

Based on the results of the previous section, one may incorrectly conclude that there is little motivation for using EPUS control, especially in conjunction with lower order Runge–Kutta schemes that show poor convergence. Although EPUS control generates smaller average errors than EPS control, such increased accuracy may appear largely unnecessary given that EPS control is already capable of maintaining the average error below the set tolerance

Table 2
Percentage of increments with errors above set integration tolerance.

Integration scheme	Error control	Percentage of increments exceeding integration tolerance set to		Average (%)
		1%	0.1%	
Modified Euler 2(1)	EPS	13.4	15.6	14.50
Runge–Kutta Nystrom 3(2)	EPS	8.0	10.0	9.00
Runge–Kutta Bogacki-Shampine 3(2)	EPS	24.8	32.8	28.80
	EPUS	1.56	2.34	1.95
Runge–Kutta 4(3)	EPS	16.6	19.1	17.85
	EPUS	0.37	0.04	0.21
Runge–Kutta Cash–Karp 5(4)	EPS	9.4	11.2	10.30
	EPUS	0.05	0.02	0.04
Runge–Kutta England 5(4)	EPS	6.9	7.6	7.25
	EPUS	0	0	0
Runge–Kutta Dormand–Prince 5(4)	EPS	3.7	4.8	4.25
	EPUS	0.02	0	0.01
Runge–Kutta Bogacki-Shampine 5(4)	EPS	10.1	22.2	16.15
	EPUS	1.75	0.98	1.37
Extrapolation	Any	0	0	0

with shorter computation times. In order to explore this conclusion further, iso-error maps have been generated, moving away from the notion of average error and investigating instead the error distribution over a domain of the strain space.

Iso-error contour plots have been produced by integrating a set of strain and suction increments of different magnitudes and directions originating from the same initial condition (i.e. mean net stress, suction and hardening parameter equal to 350 kPa, 100 kPa and 200 kPa, respectively). In particular, the Runge–Kutta and extrapolation schemes described in the companion paper [12] have been used to integrate 10,201 increments $\Delta\boldsymbol{\varepsilon}^{enh} = \{\Delta\varepsilon_s, -\Delta\varepsilon_v, \Delta s\}$ arranged over a regular square grid of 101×101 points in the strain space. Each point corresponds to increments of volumetric strain $\Delta\varepsilon_v$ and shear strain $\Delta\varepsilon_s$ equally distributed over the interval [0%, 5%] and to a constant suction increment Δs of −50 kPa. During integration of each increment, the BBM parameter values given in Table 1 were used while the error was evaluated according to Eq. (21) against a reference solution obtained by using the Runge–Kutta Cash–Karp algorithm in conjunction with a large number of equally sized subincrements (i.e. between 16,666 and 116,666 subincrements depending on the magnitude of the shear and volumetric strain increments). Such a dense grid allows an accurate description of the behaviour of the algorithms showing the true jagged nature of iso-error lines.

Table 2 compares the percentage of integration points showing maximum relative errors (i.e. the maximum of the relative errors calculated according to Eq. (21) for all net stress components) that exceed the set tolerances of 0.1% and 1%, for different integration schemes used in conjunction with both EPS and EPUS control. For the Modified Euler and Nystrom Runge–Kutta schemes, only results for the EPS control are given due to the difficulty for both these schemes to converge when used in conjunction with EPUS control.

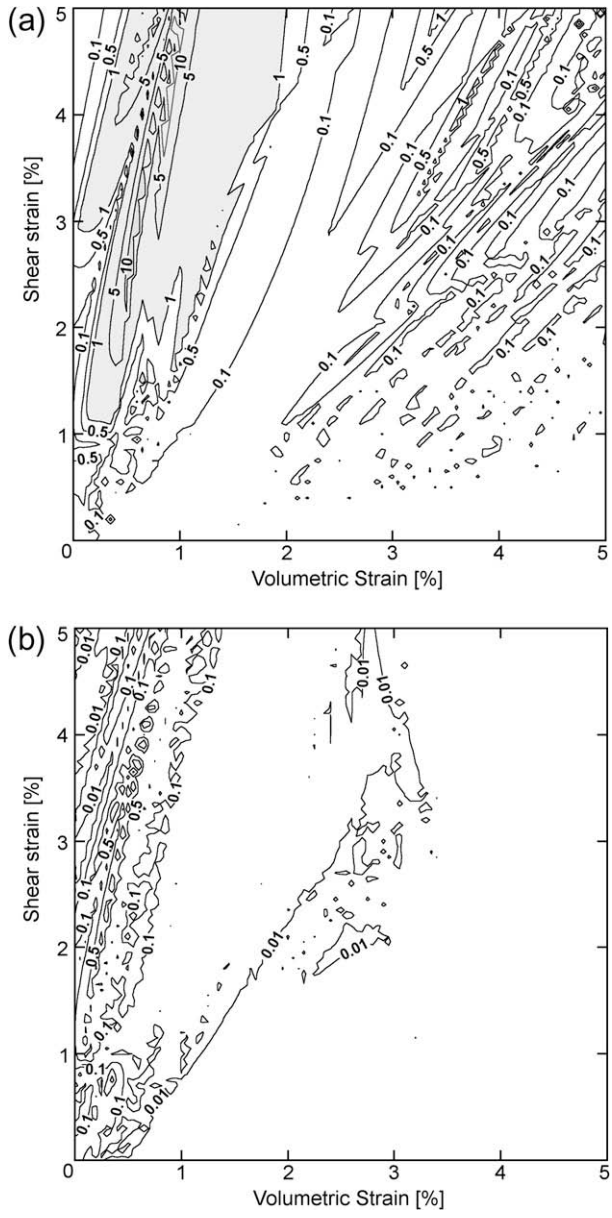

Fig. 13. Maps of maximum integration errors produced by the fourth order Runge–Kutta scheme in conjunction with: (a) EPS control and (b) EPUS control. Areas with errors larger than the set tolerance of 1% are greyed out.

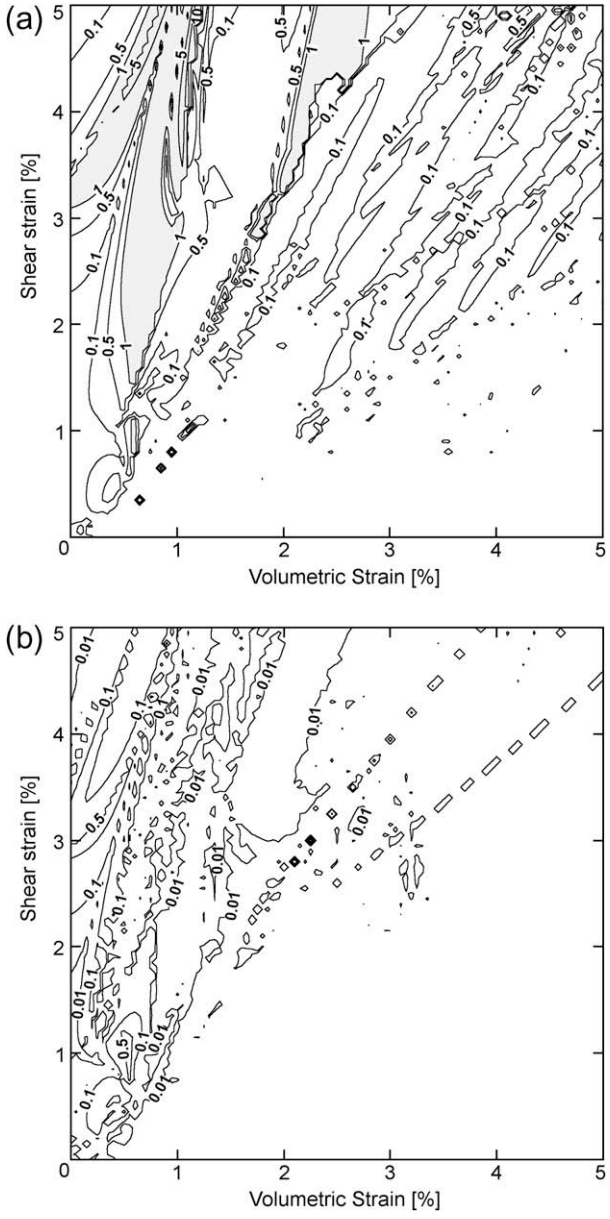

Fig. 14. Maps of maximum integration errors produced by the fifth order Runge–Kutta Cash–Karp scheme in conjunction with: (a) EPS control and (b) EPUS control. Areas with errors larger than the set tolerance of 1% are greyed out.

The error map obtained by using the Modified Euler scheme in conjunction with EPS control is shown in Fig. 12. In addition, error maps obtained by the fourth order and fifth order Cash–Karp Runge–Kutta schemes, in conjunction with both EPS and EPUS controls, are shown in Figs. 13 and 14, respectively Note that, in producing such error maps, the integration tolerance was set to 1% and the regions where the error is larger than such tolerance were greyed out.

In the previous section it has been shown that the average relative error (calculated over a large number of randomly generated increments) is always smaller than the set tolerance regardless of the error control method. However, the results given in Table 2, as well as in Figs. 12–14, indicate that the maximum relative errors for individual increments are not guaranteed to remain below the integration tolerance when EPS control is used in conjunction with Runge–Kutta schemes. In these cases, there is a sizeable proportion of increments for which integration is less accurate than required and this is true also for the most popular Modified Euler scheme (see Fig. 12 and Table 2). For the higher order Runge–Kutta schemes shown in Figs. 13 and 14, the maximum relative error can be as big as 10%, which is significantly greater than the set tolerance of 1%. On the other hand, when EPUS control is used, there are virtually no increments for which the maximum relative error exceeds the set tolerance. It is also important noting that the extrapolation scheme provides maximum relative errors that are always within the set tolerance regardless of the chosen error control.

Therefore, if Runge–Kutta schemes are used, there is a motivation for using EPUS control instead of EPS control whenever the maximum error must be maintained below the set tolerance for all integrated increments. Such greater accuracy comes, however, at the price of longer computational time and reduced algorithmic stability. In particular, if strict integration tolerances are used in conjunction with EPUS control, the Runge–Kutta schemes (especially the lower order ones) will struggle to converge.

5. Conclusions

The paper presents an investigation into the accuracy and efficiency of various algorithms for the explicit stress integration of the Barcelona Basic Model (BBM) with automatic error control. In particular, the paper presents the results obtained by using nine different integration schemes described in a companion paper [12], including eight Runge–Kutta methods of various orders as well as a novel application of the extrapolation method. The results, although strictly valid for the Barcelona Basic Model, are expected to be general and relevant to other unsaturated elastoplastic models formulated in terms of two independent stress variables, such as net stress and suction.

Initially, the results from selected integration schemes are checked against rigorous solutions of a number of BBM paths involving changes of strains and suction. Subsequently, the efficiency and accuracy of all integration schemes are assessed for generic strain increments while the difference between two alternative error control methods, i.e. the Error Per Step (EPS) method and the Error Per Unit Step (EPUS) method, is also analysed. The EPS method has been previously employed for explicit stress integration with error control of soil constitutive models. On the other hand, the EPUS method, although commonly used by applied mathematicians to enforce integration error below a set tolerance, has not been applied to stress integration in soil mechanics due to its high computational cost.

When EPS control is used, the results show that, for relatively high values of the average integration error, lower order Runge–Kutta schemes appear most efficient. However, higher order Runge–Kutta schemes tend to become progressively more competitive as the average integration error is reduced. For example, the fifth order Cash–Karp Runge–Kutta scheme shows the highest efficiency for very strict tolerances of 0.1% or lower. Overall, the third order Nystrom Runge–Kutta scheme appears the best compromise in terms of efficiency over the entire range of integration errors and may, therefore, be used as an alternative to the second order Modified Euler scheme. The use of forth and fifth order Runge–Kutta schemes, in conjunction with EPS control, is difficult to justify for standard applications where an average integration error of about 1% is acceptable, as it will result in a significant increase of calculation time compared to second and third order Runge–Kutta schemes. The extrapolation method shows excellent stability but it requires long computational times and might be used as a back-up integration method when Runge–Kutta schemes fail to converge.

When EPUS control is employed, the use of higher order Runge–Kutta methods is necessary over the entire range of integration errors to ensure acceptable levels of efficiency and robustness. Tests performed in this work suggest that the fifth order Cash–Karp scheme is the most efficient choice closely trailed by other fifth order schemes. The differences between these schemes are not very significant and other higher order schemes would probably perform equally well. The extrapolation method, thanks to its superior stability, may also be used as an alternative integration method when Runge–Kutta schemes show poor convergence.

Both EPUS and EPS methods generate average relative integration errors (computed over a large number of integration increments) that are significantly lower than the set tolerance for all integration schemes. Nevertheless, Runge–Kutta schemes must be used in conjunction with EPUS control, rather than EPS control, if the integration error for each individual increment (not only the average integration error) must remain below the set tolerance. This higher level of accuracy of EPUS control comes at the price of relatively poor convergence and long computational times especially when lower order Runge–Kutta schemes are used and strict values of the integration tolerance are set. When strict integration tolerances must be enforced in all increments, the choice of the extrapolation scheme may be advisable instead. In addition to its robustness and stability, the extrapolation scheme offers the best error control properties among all algorithms tested, though it requires longer computational times. If the extrapolation scheme is used, the choice of the error control method becomes largely irrelevant as both accuracy and computational efficiency remain virtually unchanged regardless of whether EPS or EPUS control is employed.

Acknowledgements

The authors gratefully acknowledge funding by the European Commission through the MUSE Research Training Network, Contract: MRTN-CT-2004-506861.

References

[1] Alonso EE, Gens A, Josa A. A constitutive model for partially saturated soils. Géotechnique 1990;40(3):405–30.
[2] Bogacki P, Shampine LF. An efficient Runge–Kutta (4, 5) pair. Comput Math Appl 1996;32(6):15–28.
[3] Deuflhard P, Bornemann F. Scientific computing with ordinary differential equations. Text in applied mathematics 42. Springer; 2002.
[4] Dormand JR. Numerical methods for differential equations. A computational approach. Boca Raton: CRC Press; 1996.
[5] Lee HJ, Schiesser WE. Ordinary and partial differential equation routines in C, C++, Fortran, Java, Maple, and Matlab. Boca Raton: CRC Press; 2003.
[6] Potts DM, Zdravkovic L. Finite element analysis in geotechnical engineering: theory. London: Thomas Telford Publishing; 1999.
[7] Press WH, Teukolsky SA, Vetterling WT, Flannery BP. Numerical recipes in C++. The art of scientific computing. Cambridge: University Press; 2002.

[8] Shampine LF. Numerical solution of ordinary differential equations. New York: Chapman & Hall; 1994.
[9] Sheng D, Sloan SW, Gens A, Smith DW. Finite element formulation and algorithms for unsaturated soils. Part II: verification and application. Int J Numer Anal Meth Geomech 2003;27:767–90.
[10] Sloan SW. Substepping schemes for the numerical integration of elastoplastic stress–strain relations. Int J Numer Method Eng 1987;24:893–911.
[11] Sołowski WT, Gallipoli D. Numerical integration of elasto-plastic constitutive models using the extrapolation method. In: Pande, Pietruszczak, editors. Proceeding of the NUMOG X conference, Rhodes. Greece, 25–27 April 2007, Taylor & Francis Group; 2007. p. 211–7.
[12] Sołowski WT, Gallipoli D. Explicit stress integration with error control for Barcelona Basic Model. Part I: algorithms formulation. Comput Geotech 2010;37(1/2):59–67.